Atmospheric dynamics feedback: concept, simulations and climate implications

Michael P. Byrne*

Imperial College London, London, United Kingdom

Tapio Schneider

California Institute of Technology, Pasadena, California

Corresponding author address: Michael P. Byrne, Space and Atmospheric Physics Group, Imperial College London, London SW7 2AZ, United Kingdom

E-mail: michael.byrne@imperial.ac.uk

ABSTRACT

The regional climate response to radiative forcing is largely controlled by changes in the atmospheric circulation. It has been suggested that global climate sensitivity also depends on the circulation response, an effect we call the "atmospheric dynamics feedback". Using a technique to isolate the influence of changes in atmospheric circulation on top-of-atmosphere radiation, we calculate the atmospheric dynamics feedback in coupled climate models. Large-scale circulation changes contribute substantially to all-sky and cloud feedbacks in the tropics but are relatively less important at higher latitudes. Globally averaged, the atmospheric dynamics feedback is positive and amplifies the near-surface temperature response to climate change by an average of 8% in simulations with coupled models. A constraint related to the atmospheric mass budget results in the dynamics feedback being small on large scales relative to feedbacks associated with thermodynamic processes. Idealized-forcing simulations suggest that circulation changes at high latitudes are potentially more effective at influencing global temperature than circulation changes at low latitudes, and the implications for past and future climate change are discussed.

1. Introduction

The general circulation of the atmosphere is expected to change in a variety of ways as climate warms in response to CO_2-induced radiative forcing. Projected circulation responses include a widening of the Hadley circulation (Lu et al. 2007), a narrowing of the intertropical convergence zone (ITCZ) (Byrne and Schneider 2016b), a slowdown in the Walker circulation (Vecchi and Soden 2007), and a poleward shift of the mid-latitude storm tracks (Yin 2005; Schneider et al. 2010). Regional climate change, including projected changes in the water cycle, is strongly dependent on these circulation responses (e.g., Seager et al. 2010; Scheff and Frierson 2012; Shepherd 2014; Byrne and O'Gorman 2015). Not only does the circulation affect *regional* climate but it has also been suggested that *global* climate change may be amplified or dampened by the atmospheric circulation response via its effect on the planetary radiation budget (e.g., Pierrehumbert 1995); we refer to this effect as the "atmospheric dynamics feedback".

Studies of how atmospheric circulation responses to global warming affect top-of-atmosphere (TOA) radiation and climate have largely focused on interactions between the tropical circulation and clouds (Lindzen et al. 2001; Bony et al. 2004; Wyant et al. 2006; Mauritsen and Stevens 2015; Bony et al. 2016). The 'iris' hypothesis of Lindzen et al. (2001) argued that a decrease in the portion of the tropics covered by high clouds and a concurrent increase in low-cloud area under global warming is an important negative feedback on climate change. Pierrehumbert (1995) put forward a similar mechanism as a potential means of regulating tropical sea-surface temperatures in warm climates of the past (e.g., the Eocene). The physics of this proposed negative feedback are intuitive and rely on differences in cloud-radiative effect between low-cloud and high-cloud regions. The shortwave and longwave cloud-radiative effects are defined conventionally as the differences between the clear-sky outgoing shortwave or longwave fluxes at TOA and the all-

sky outgoing fluxes (Allan 2011). Specifically, the shortwave cloud-radiative effect is $SW^{\mathrm{TOA}}_{\mathrm{clear}} \uparrow - SW^{\mathrm{TOA}}_{\mathrm{all}} \uparrow$, and the longwave cloud-radiative effect is $LW^{\mathrm{TOA}}_{\mathrm{clear}} \uparrow - LW^{\mathrm{TOA}}_{\mathrm{all}} \uparrow$, where SW and LW indicate the longwave and shortwave TOA fluxes, respectively, and $\uparrow$ denotes an upward flux. Low clouds have a negative cloud-radiative effect and cool the Earth because they reflect incoming shortwave radiation while having only a weak longwave greenhouse effect. High clouds, on the other hand, typically have a small cloud-radiative effect because of a large cancellation between shortwave cooling and longwave warming (Ramanathan et al. 1989). Consequently, a decrease in the area of high clouds (with small cloud-radiative effect) and an increase in the area of strongly cooling low clouds under global warming is a possible negative feedback on climate change.

Although the validity of the original iris hypothesis proposed by Lindzen et al. (2001) has been strongly challenged (e.g., Fu et al. 2002), recent studies have revived interest in iris-type phenomena as potentially important feedbacks on climate change (Mauritsen and Stevens 2015; Bony et al. 2016; Cronin and Wing 2017). The suggestion that tropical convection will become more aggregated as sea-surface temperatures increase (e.g., Wing and Emanuel 2014) has formed the conceptual basis for these 'iris 2.0' studies. Convective aggregation is not typically simulated by global climate models, in which convection is parameterized out of necessity, but it has been put forward as a negative iris-type atmospheric dynamics feedback (Bony et al. 2016; Wing et al. 2017; Cronin and Wing 2017). Perhaps related to convective aggregation, a narrowing of tropical high-cloud regions (i.e., the ITCZ) relative to neighboring low-cloud regions under global warming has been observed over recent decades (Wodzicki and Rapp 2016) and further narrowing is expected as the climate continues to warm (Lau and Kim 2015; Byrne and Schneider 2016b). This ITCZ narrowing represents another potential iris effect. At higher latitudes, cloud feedbacks associated with shifts in the extratropical circulation have received considerable attention in re-

cent years (Grise et al. 2013; Kay et al. 2014; Wall and Hartmann 2015), though climate models disagree on the magnitude and importance of these feedbacks (Ceppi et al. 2017a).

The studies mentioned above focus on cloud feedbacks, but it is plausible that a re-organization of the atmospheric circulation could also affect the water-vapor feedback by changing the spatial pattern and intensities of moisture convergence and divergence zones. More generally, atmospheric circulation changes can conceivably influence both the cloud-radiative effect and all-sky TOA radiative fluxes at all latitudes, but the magnitudes of these atmospheric dynamics feedbacks and their dependences on latitude are unknown. Are there latitudes at which climate feedbacks are dominated by large-scale circulation changes? How do these circulation changes contribute to global climate change? Can our emerging understanding of atmospheric dynamics in a changing climate be used to better constrain global climate sensitivity? Are low-latitude or high-latitude circulation changes more effective at changing global-mean surface temperature? Related to this latter question, a number of studies have shown that the spatial pattern of ocean heat uptake strongly affects the global temperature response (Armour et al. 2013; Rose et al. 2014; Rugenstein et al. 2016), i.e., heat absorbed by the ocean at high latitudes has a stronger effect on global temperature than the same quantity of heat absorbed at low latitudes. Should such a latitudinal dependence also exist for the atmospheric dynamics feedback, it would have important implications for the ability of tropical iris-type mechanisms to regulate past and future climate change.

Here we use coupled climate models together with idealized simulations to assess how large-scale atmospheric circulation changes contribute to TOA radiative feedbacks and global climate change. We begin by outlining the method used to decompose dynamic versus thermodynamic influences on TOA radiation (Section 2) before analysing the atmospheric dynamics feedback in simulations with coupled models (Section 3). Idealized simulations with stylized TOA radiative forcings are also performed to understand how circulation changes at different latitudes could

influence global climate (Section 4). We conclude by summarizing our results and discussing directions for future research (Section 5).

2. Estimating the atmospheric dynamics feedback

a. CMIP5 simulations

We will investigate the role of the atmospheric circulation in controlling radiative feedbacks using simulations from the Coupled Model Intercomparison Project Phase 5 (CMIP5) (Taylor et al. 2012). In particular, we analyze changes in TOA radiative fluxes for 27 models[1] between pre-industrial control runs (*piControl*) and runs in which the CO_2 concentration is instantaneously quadrupled relative to pre-industrial levels (*abrupt4xCO2*). For both the *piControl* and *abrupt4xCO2* runs, we analyze 100 years of monthly-mean data. All-sky and clear-sky TOA radiative fluxes are defined as positive downwards.

b. Dependence of top-of-atmosphere radiation on the atmospheric circulation

To estimate the radiative feedbacks associated with changes in the large-scale atmospheric circulation, we first decompose TOA radiative anomalies (e.g., due to changes in greenhouse gas concentrations) into "dynamic", "thermodynamic", and "nonlinear" components (where nonlinear here means the combined influence of changes in dynamic and thermodynamic processes on TOA radiation). To perform this decomposition, we follow Bony et al. (2004) in using the mid-tropospheric vertical velocity, ω, as an admittedly imperfect proxy for dynamical effects. That

[1]The models analyzed in this study are: ACCESS1-0, ACCESS1-3, BCC-CSM1-1, BCC-CSM1-1-M, CanESM2, CCSM4, CNRM-CM5, CNRM-CM5-2, CSIRO-Mk3-6-0, FGOALS-g2, FGOALS-s2, GFDL-CM3, GFDL-ESM2G, GFDL-ESM2M, GISS-E2-H, GISS-E2-R, HadGEM2-ES, INMCM4, IPSL-CM5A-LR, IPSL-CM5B-LR, MIROC5, MIROC-ESM, MPI-ESM-LR, MPI-ESM-MR, MPI-ESM-P, MRI-CGCM3, and NorESM1-M

is, we decompose changes in TOA fluxes into those that are, and are not, associated with vertical velocity changes.

To estimate how changes in atmospheric circulation affect the TOA radiative response to an imposed forcing, we first construct discretized functions $R_{\text{cloud}}(\omega,\phi)$ and $R_{\text{all}}(\omega,\phi)$ at each latitude ϕ, where $R_{\text{cloud}}(\omega,\phi)$ is the cloud-radiative effect and $R_{\text{all}}(\omega,\phi)$ is the all-sky TOA radiative flux, and both quantities are 'binned' as a function of mid-tropospheric vertical velocity. The radiative fluxes and vertical velocities used in our analysis are all monthly-mean quantities. We also construct normalized area probability density functions (PDFs) for vertical velocity at each latitude, $A(\omega,\phi)$. Note that $R_{\text{cloud}}(\omega,\phi)$, $R_{\text{all}}(\omega,\phi)$, and $A(\omega,\phi)$ (and the radiative anomalies and feedbacks discussed below) are calculated for each CMIP5 model individually before being linearly interpolated to a common grid for the purpose of plotting multimodel means as a function of latitude. In this framework, the zonally-averaged cloud-radiative effect or all-sky TOA flux [$\overline{R_{\text{cloud}}}(\phi)$ or $\overline{R_{\text{all}}}(\phi)$] is the product of $R_{\text{cloud}}(\omega,\phi)$ or $R_{\text{all}}(\omega,\phi)$ with $A(\omega,\phi)$ at latitude ϕ integrated over all vertical-velocity bins, which in continuous form are expressed as:

$$\overline{R_{\text{cloud}}}(\phi) = \int_{-\infty}^{\infty} R_{\text{cloud}}(\omega,\phi)A(\omega,\phi)d\omega \tag{1}$$

$$\overline{R_{\text{all}}}(\phi) = \int_{-\infty}^{\infty} R_{\text{all}}(\omega,\phi)A(\omega,\phi)d\omega, \tag{2}$$

where $\overline{(\cdot)}$ denotes an area-weighted integral over vertical velocity. The $R_{\text{cloud}}(\omega,\phi)$, $R_{\text{all}}(\omega,\phi)$, and $A(\omega,\phi)$ functions for the *piControl* runs are constructed for each climatological month using 100 years of monthly-mean simulation data. These functions are then re-calculated for each month and year in the *abrupt4xCO2* runs to quantify [using the decompositions (4) and (5) described below] how dynamic and thermodynamic processes contribute to the radiative feedbacks that determine Earth's response to a quadrupling of CO_2.

The dependence of tropical cloud-radiative effect on vertical velocity (Fig. 1a) and the area PDF of vertical velocity (Fig. 1d) in one coupled climate model are similar to the observed functions [cf. Fig. 2 in Bony et al. (2004)]. Note that in Figure 1, each quantity has been averaged from $\phi = -30^\circ$ to 30° with area weighting. Between ascending ($\omega < 0$) and weakly descending ($\omega > 0$) regions, the longwave and shortwave cloud-radiative effects vary approximately linearly with mid-tropospheric vertical velocity (Fig. 1a). For the longwave cloud-radiative effect, the positive (i.e., heating) values in strongly ascending regions such as the ITCZ reflect cold, high-altitude cloud tops and large cloud fractions, which together produce a strong greenhouse effect. The decreasing longwave cloud-radiative effect with increasing ω (i.e., weaker upward motion) is due to cloud-top altitudes and cloud fractions declining for weaker ascent regimes. For the shortwave cloud-radiative effect (Fig. 1a), the reduced cooling as ascending motion weakens is a result of decreasing cloud fractions and less shortwave reflection to space. The relative insensitivity of the longwave and shortwave cloud-radiative effects to changes in vertical velocity in strongly descending regions is likely due to cloud-masking effects (Soden et al. 2004). It shows that the altitude and fraction of low clouds in such regions no longer depend strongly on mid-tropospheric vertical velocity (Bony et al. 2004).

Although we would not necessarily expect the dependence of clear-sky radiative fluxes on vertical velocity to be as strong as that found for the cloud-radiative effect, it is plausible that regions of low-level convergence would be moister than regions of divergence, which would have a signature in the clear-sky radiative flux and contribute to an all-sky flux dependence on vertical velocity. Indeed tropical ascending regions are observed to have smaller clear-sky longwave cooling relative to descending regions (Bony et al. 1997); this clear-sky flux dependence on vertical velocity is at least qualitatively captured by climate models (Fig. 1b). There is also a simulated dependence of clear-sky shortwave radiation on vertical velocity (Fig. 1b), with regions of descent generally

having a larger outgoing shortwave flux and a stronger longwave radiative cooling (presumably because the atmosphere in these descending regions is dry and consequently absorbs less shortwave radiation, for example above deserts such as the Sahara). The influence of vertical velocity on clear-sky fluxes and on the cloud-radiative effect combine to produce a strong dependence of all-sky fluxes on vertical velocity, particularly the longwave fluxes (Fig. 1c). Figure 1 shows the relationships of cloud-radiative effect, clear-sky fluxes, and all-sky fluxes to vertical velocity for one climate model, but these relationships are qualitatively similar for the other 26 models analyzed (not shown).

The area PDF of vertical velocity in a climate model shows a skewed distribution in the tropics (Fig. 1d), with a large area covered by slow-moving descending air masses — the so-called 'radiator fin' regions where longwave cooling is strong (Pierrehumbert 1995). The area PDF has a relatively small ascent region with a larger variance in vertical velocity compared to the descent region (Fig. 1d), and is qualitatively similar to a PDF calculated using reanalysis data (Bony et al. 2004).

c. Dynamic/thermodynamic decomposition of changes in top-of-atmosphere radiation

Our objective is to identify the roles of dynamic versus thermodynamic processes in controlling the *response* of TOA radiation to an imposed $4 \times CO_2$ forcing, i.e., we want to estimate the atmospheric dynamics and thermodynamics feedbacks. Consequently, before applying the decomposition method of Bony et al. (2004), we first need to estimate and remove the component of the TOA radiative anomalies associated with the imposed forcing. To do this, we consider a linearization of the TOA radiation budget which is typically invoked to describe global climate change (e.g., Armour et al. 2013):

$$[\delta R_{\text{all}}]^g = [F]^g + [\lambda_{\text{all}}]^g [\delta T]^g, \tag{3}$$

where δR_{all} denotes the all-sky TOA radiative imbalance (or anomaly) in units of $\mathrm{W\,m^{-2}}$, F is the imposed radiative forcing ($\mathrm{W\,m^{-2}}$), λ_{all} is the all-sky feedback parameter ($\mathrm{W\,m^{-2}\,K^{-1}}$), δT is the surface-air temperature response (K), δ indicates an anomaly (or change) between the *pi-Control* and *abrupt4xCO2* runs, and $[\cdot]^g$ denotes a global average. The all-sky feedback parameter quantifies the efficiency with which the Earth system equilibrates a radiative forcing. In this linear framework, the radiative response of the climate system to the imposed forcing is obtained by subtracting the forcing from the total TOA radiative anomaly, i.e., $[\delta R'_{\text{all}}]^g \equiv [\delta R_{\text{all}}]^g - [F]^g$ where $\delta R'_{\text{all}}$ is defined to be the *all-sky radiative response*.

The dynamic components of the (i) all-sky radiative response or (ii) changes in cloud-radiative effect are identified as the TOA radiative anomalies induced by changes in $A(\omega,\phi)$ for (i) fixed $R_{\text{all}}(\omega,\phi)$ or (ii) fixed $R_{\text{cloud}}(\omega,\phi)$. The decompositions are expressed mathematically as:

$$\begin{aligned}\overline{\delta R'_{\text{all}}}(\phi) = &\underbrace{\int_{-\infty}^{\infty} R_{\text{all}}(\omega,\phi)\delta A(\omega,\phi)d\omega}_{\text{dynamic}} + \underbrace{\int_{-\infty}^{\infty} [\delta R_{\text{all}}(\omega,\phi) - F(\phi)]A(\omega,\phi)d\omega}_{\text{thermodynamic}} \\ &+ \underbrace{\int_{-\infty}^{\infty} [\delta R_{\text{all}}(\omega,\phi) - F(\phi)]\delta A(\omega,\phi)d\omega}_{\text{nonlinear}} \end{aligned} \tag{4}$$

$$\begin{aligned}\overline{\delta R_{\text{cloud}}}(\phi) = &\underbrace{\int_{-\infty}^{\infty} R_{\text{cloud}}(\omega,\phi)\delta A(\omega,\phi)d\omega}_{\text{dynamic}} + \underbrace{\int_{-\infty}^{\infty} \delta R_{\text{cloud}}(\omega,\phi)A(\omega,\phi)d\omega}_{\text{thermodynamic}} \\ &+ \underbrace{\int_{-\infty}^{\infty} \delta R_{\text{cloud}}(\omega,\phi)\delta A(\omega,\phi)d\omega}_{\text{nonlinear}} \end{aligned} \tag{5}$$

where $\overline{\delta R'_{\text{all}}}(\phi)$ is the total (shortwave + longwave) all-sky radiative response at latitude ϕ averaged over all vertical velocities with area weighting (note that the forcing is removed on the right-hand side), $\overline{\delta R_{\text{cloud}}}(\phi)$ is the change in cloud-radiative effect, and $F(\phi)$ is the diagnosed radiative forcing (see Section 2d for details regarding the calculation of the forcing), and $\delta A(\omega,\phi)$ is the change in the normalized area PDF of vertical velocity. The anomalies $\overline{\delta R'_{\text{all}}}(\phi)$ and $\overline{\delta R_{\text{cloud}}}(\phi)$

are calculated by evaluating the changes in radiative fluxes in each of the first 100 years of the *abrupt4xCO2* simulations relative to the climatological fluxes from the *piControl* simulations. By construction, the decompositions (4) and (5) match the simulated all-sky radiative responses and changes in cloud-radiative effects very accurately (not shown).

In general, the dynamic components of (4) and (5) could be due to changes in the areas occupied by ascending versus descending air (e.g., a narrowing of the ITCZ), strengthening/weakening of the circulations within the ascending and descending regimes (e.g., a slowdown of the Walker circulation), or spatial shifts in circulation features (e.g., a poleward movement of the storm track). It should be noted that dynamic processes, for example lower-tropospheric mixing or convective mass fluxes, that might be de-coupled from mid-tropospheric vertical velocity or which are not explicitly resolved by global climate models, do not form part of what we define as the (large-scale) dynamic components and are instead included in the thermodynamic components (Wyant et al. 2006). The thermodynamic components represent the portion of the all-sky radiative response or the change in cloud-radiative effect that would occur if the atmospheric circulation did not change [i.e., for fixed $A(\omega,\phi)$], and includes effects such as changes in cloud optical depth and increases in water-vapor concentration that accompany a warming atmosphere. The nonlinear component represents the combined effect of changes in dynamic and thermodynamic processes. We apply this decomposition not only to changes in the cloud-radiative effect as in Bony et al. (2004), but also to the all-sky radiative response.

Our method of evaluating (4) and (5) differs from that of Bony et al. (2004) in a number of respects. Firstly, we perform the decomposition over the whole globe, not only for tropical regions, and construct the $R_{\mathrm{all}}(\omega,\phi)$ and $R_{\mathrm{cloud}}(\omega,\phi)$ functions and the area PDFs using a vertically-averaged vertical velocity between 400 hPa and 500 hPa (our results are qualitatively similar when we average vertical velocity over the full atmosphere). Secondly, to understand how circulation

changes at different latitudes contribute to the atmospheric dynamics feedback, we perform the decomposition at each latitude individually rather than over a large region. If the cloud-radiative effect and all-sky radiative flux were solely functions of vertical velocity, then it would be possible to construct $R_{\rm all}$ and $R_{\rm cloud}$ using global data and then trace back to latitude to understand the influence of circulation changes in different regions on TOA radiation. However, TOA radiation depends not only on vertical velocity but also on temperature, relative humidity, solar zenith angle, surface albedo, and other factors. Consequently, building $R_{\rm all}$ and $R_{\rm cloud}$ functions using global data and then using these functions to determine dynamics and thermodynamics feedbacks at a particular latitude is not possible as the local TOA radiation budget does not close.

When performing the decompositions (4) and (5), the vertical-velocity limits of $R_{\rm all}(\omega,\phi)$, $R_{\rm cloud}(\omega,\phi)$, and $A(\omega,\phi)$ are specified to be the maximum and minimum values of the vertically-averaged vertical velocity at each latitude, and we use 21 equally-spaced vertical-velocity 'bins'. If there are bins that are empty when constructing $R_{\rm all}(\omega,\phi)$, $R_{\rm cloud}(\omega,\phi)$, and $A(\omega,\phi)$, we use linearly interpolated forms of these functions for which the missing values are filled in when calculating the various terms in (4) and (5). We now use these decompositions to estimate the climate feedbacks associated with dynamic and thermodynamic processes.

d. Feedback calculation

We define the dynamics, thermodynamics, and nonlinear all-sky and cloud feedbacks at each latitude to be the respective components of the all-sky radiative response (4) or changes in cloud-radiative effect (5) at that latitude normalized by the global-mean surface-air temperature change [feedbacks are conventionally defined in climate science as TOA radiative responses normalized

by the surface temperature change (e.g., Rose and Rayborn 2016)]:

$$\lambda_{\text{all}}(\phi) = \lambda_{\text{all}}^{\text{dy}}(\phi) + \lambda_{\text{all}}^{\text{th}}(\phi) + \lambda_{\text{all}}^{\text{nl}}(\phi) \tag{6}$$

$$\lambda_{\text{cloud}}(\phi) = \lambda_{\text{cloud}}^{\text{dy}}(\phi) + \lambda_{\text{cloud}}^{\text{th}}(\phi) + \lambda_{\text{cloud}}^{\text{nl}}(\phi), \tag{7}$$

where λ_{all} is the all-sky feedback, λ_{cloud} is the cloud feedback, and the labels "dy", "th", and "nl" denote the dynamic, thermodynamic, and nonlinear components of each feedback, respectively. Our focus in this study is the atmospheric dynamics feedback, which we define to be the $\lambda_{\text{all}}^{\text{dy}}(\phi)$ component; we will also discuss the dynamic component of the cloud feedback, $\lambda_{\text{cloud}}^{\text{dy}}(\phi)$. The global average of the all-sky feedback is simply the global feedback parameter defined in (3). The various components of the all-sky (6) and cloud feedbacks (7) are estimated for each climate model individually using ordinary least-squares regressions of the dynamic, thermodynamic, and nonlinear components of $\overline{\delta R'_{\text{all}}}(\phi)$ and $\overline{\delta R_{\text{cloud}}}(\phi)$ versus global-mean surface-air temperature changes following CO_2 quadrupling (all anomalies in these regressions are with respect to the 100-year climatological averages from the *piControl* runs). The intercepts of the regressions of $\overline{\delta R_{\text{all}}}(\phi)$ versus global-mean surface-air temperature at each latitude are defined as the 'adjusted' radiative forcings, $F(\phi)$ (Andrews et al. 2012). We use 100 years of simulation data following CO_2 quadrupling in these regressions and note that this method includes rapid climate adjustments as part of the climate feedback. In the next section, we will compare the influences of rapid circulation adjustments versus slower, temperature-mediated adjustments on the radiative response.

3. Atmospheric dynamics feedback in coupled climate models

a. Feedbacks versus latitude

The multimodel-mean all-sky and cloud feedbacks in the *abrupt4xCO2* simulations are plotted in Figure 2, along with the thermodynamic, dynamic, and nonlinear components of these feed-

backs. The nonlinear component is substantially smaller than the dynamic component so for simplicity we will mostly show the sum of the dynamic and nonlinear components rather than each individually (a discussion of the factors controlling the magnitude of the nonlinear component is provided later in this section).

1) ALL-SKY AND CLOUD FEEDBACKS

As expected, the total all-sky feedback is negative (i.e., decreasing net downward radiation at TOA as climate warms) at all latitudes (Fig. 2a). The thermodynamic component typically dominates the all-sky feedback but the dynamic component is substantial in the tropics, where its magnitude is up to half of the magnitude of the thermodynamics feedback. Changes in large-scale circulation produce a positive dynamics feedback close to the equator (the opposite of a negative iris feedback) and contribute $+0.5\,\mathrm{W\,m^{-2}}$ per degree global warming to the TOA imbalance in that region. The positive all-sky dynamics feedback in the deep tropics is a result of cloud (Fig. 2b) and clear-sky feedbacks (not shown), and extends into the Southern Hemisphere subtropics, though the magnitude is smaller than in the deep tropics. In the Northern Hemisphere subtropics, the dynamics feedback is more complex, with a positive-negative dipole between 10°N and 30°N (Fig. 2a).

The latitudinal structure of the dynamics feedback broadly reflects changes in mid-tropospheric vertical velocity (Fig. 3): A strengthening of ascent in the core of the ITCZ under global warming intensifies moisture convergence in that region, which increases atmospheric water vapor and enhances the longwave greenhouse effect (Fig. 4a,b). These positive longwave all-sky and cloud feedbacks in the ITCZ are caused by strengthening ascent and moisture convergence in the middle of the ITCZ with warming (Byrne and Schneider 2016b) and an upward shift in the altitude of high clouds (Zelinka et al. 2012), which together produce a large and positive dynamics feedback on

the equator (Fig. 2a). The extent to which this dynamical longwave cloud feedback is consistent with the fixed anvil temperature (FAT) hypothesis of Hartmann and Larson (2002) is a topic for future work. The all-sky longwave feedback in the core of the ITCZ is counteracted somewhat by a smaller negative shortwave feedback (Fig. 4a). This shortwave feedback is predominantly associated with cloud processes (Fig. 4b) and points to increases in cloud fraction, thickness, and albedo in the core of the ITCZ because of the strengthening and narrowing of the ascent in that region; this pattern of tropical circulation changes has been termed the "deep-tropics squeeze" (Lau and Kim 2015).

Moving from the core of the ITCZ to its equatorward flanks and into the subtropics, the longwave and shortwave components of the dynamics feedback change signs and tend to largely cancel one another (Fig. 4). The weakening of ascending motion on the equatorward flanks of the climatological ITCZ following CO_2 quadrupling (Fig. 3) causes reduced moisture convergence in those regions and negative longwave clear-sky and cloud feedbacks; changes in free-tropospheric clouds associated with a narrowing of the ITCZ are also likely to contribute to this negative longwave feedback. The longwave feedbacks are mostly cancelled by positive shortwave feedbacks at the edges of the ITCZ and in the subtropics, and these shortwave components are also dominated by cloud feedbacks (Fig. 4b). The positive shortwave cloud feedback in this region reflects a decrease in the amount of shallow marine cloud with global warming (Bony and Dufresne 2005), though the physical processes driving these changes in low-cloud amount are neither well understood nor well represented in global climate models (Ceppi et al. 2017a). Because of the strong cancellation between longwave and shortwave feedbacks on the equatorward flanks of the ITCZ and in the subtropics, the overall all-sky dynamics feedback in this region is smaller than in the core of the ITCZ (Fig. 4a).

2) Fast versus slow dynamic responses

Cloud-radiative feedbacks are typically divided into 'cloud adjustments', which emerge rapidly in response to a radiative forcing, and surface temperature-mediated changes, which evolve slowly as the climate warms (Andrews et al. 2012; Kamae et al. 2015). The dynamic components of $\overline{\delta R'_{\mathrm{all}}}(\phi)$ and $\overline{\delta R_{\mathrm{cloud}}}(\phi)$ also have fast and slow components (Fig. 5a,c). Poleward of approximately 30°, the dynamic components are very similar in the first year ("fast") and averaged over years 91-100 ("slow") following the quadrupling of CO_2. Equatorward of 30°, however, there are considerable differences between the fast and slow dynamic responses. In the deep tropics, close to the equator, both the all-sky (Fig. 5a) and cloud-radiative dynamic responses (Fig. 5c) are strongly positive (warming) 91-100 years after CO_2 quadrupling but are much smaller and negative in the first year. This slow response is consistent with the ascent at the core of the ITCZ intensifying considerably between the two time periods analyzed (not shown). The thermodynamic components of $\overline{\delta R'_{\mathrm{all}}}(\phi)$ and $\overline{\delta R_{\mathrm{cloud}}}(\phi)$ emerge much more slowly (Fig. 5b,d), as expected by definition of the thermodynamic components as being controlled by temperature changes.

The vertically-integrated atmospheric moist static energy (MSE) budget can be used diagnostically to understand the physical processes influencing tropical vertical velocity (Byrne and Schneider 2016a). Changes in the net energy input to the atmosphere (e.g., through TOA radiative anomalies) influence the MSE budget and consequently vertical velocity, and can be a fast response to CO_2 forcing. On the other hand, poleward transport of MSE by large-scale mean advection and transient eddies also affects tropical vertical velocity and depends fundamentally on meridional MSE gradients (Byrne and Schneider 2016a); these gradients would be expected to evolve slowly in response to CO_2 forcing as sea-surface temperatures increase. It is unclear why the dynamic components of changes in cloud-radiative effect [$\overline{\delta R_{\mathrm{cloud}}}(\phi)$] and all-sky radiative

response [$\overline{\delta R'_{\mathrm{all}}(\phi)}$] evolve on different timescales at low and high latitudes [Ceppi et al. (2017b) find a similar latitudinal dependence of timescales] – this is a topic for future work. The different circulation-response timescales at different latitudes will be shown later to influence the global feedback parameter and the response of the Earth system to CO_2 forcing.

Finally, there is only a weak correlation across CMIP5 models between the globally-averaged fast and slow dynamic components of the all-sky radiative response ($r = 0.38$). This weak relationship casts doubt on the feasibility of using the fast component to understand the long-term influence of changes in atmospheric circulation on TOA radiation. This contrasts with the fast and slow responses of tropical precipitation changes, which have been shown to be strongly determined by the fast circulation response (Bony et al. 2013).

3) "AREA" AND "MIX" COMPONENTS OF THE DYNAMICS FEEDBACK

In an influential paper on the energetics of tropical climate, Pierrehumbert (1995) used a simple two-box model to argue that "the warm pool sea surface temperature is very sensitive to [...] the relative area of the dry versus convective regions". Expressed in an equivalent way, Pierrehumbert (1995) was suggesting that the ratio of the areas of tropical ascent versus descent regions is an important controller of tropical climate. A widening of the Hadley circulation and a narrowing of the ITCZ are expected to occur as climate warms, resulting in a decrease in the area of tropical ascent relative to the area of tropical descent (Byrne and Schneider 2016b). We have calculated the total dynamics feedback, but it is also of interest to isolate the portion of this feedback that is due to a change in the up-down area ratio (e.g., due to ITCZ narrowing) and the portion that is due to strengthening/weakening of the circulation within the distinct ascent and descent regimes (e.g., due to a slowdown of the Walker circulation).

We decompose each of the all-sky and cloud dynamics feedbacks, $\lambda_{\text{all}}^{\text{dy}}(\phi)$ and $\lambda_{\text{cloud}}^{\text{dy}}(\phi)$, into two parts: The first part, the "area component" $\lambda_{\text{area}}^{\text{dy}}(\phi)$, corresponds to changes in the up-down area ratio and the second part, the "mix component" $\lambda_{\text{mix}}^{\text{dy}}(\phi)$, corresponds to changes in the vertical-velocity distribution within the ascent and descent regimes. The two components of the all-sky dynamics feedback are expressed mathematically as follows:

$$\begin{aligned}\lambda_{\text{all}}^{\text{dy}}(\phi) &= \lambda_{\text{area}}^{\text{dy}}(\phi) + \lambda_{\text{mix}}^{\text{dy}}(\phi) \\ &= \underbrace{\left(\int_{-\infty}^{0} [R_{\text{all}}]^{\text{u}}[\delta A]^{\text{u}} d\omega + \int_{0}^{\infty} [R_{\text{all}}]^{\text{d}}[\delta A]^{\text{d}} d\omega\right) / [\delta T]^{g}}_{\text{area component}} + \\ &\underbrace{\left(\int_{-\infty}^{0} (R_{\text{all}} - [R_{\text{all}}]^{\text{u}})(\delta A - [\delta A]^{\text{u}}) d\omega + \int_{0}^{\infty} (R_{\text{all}} - [R_{\text{all}}]^{\text{d}})(\delta A - [\delta A]^{\text{d}}) d\omega\right) / [\delta T]^{g}}_{\text{mix component}}\end{aligned} \tag{8}$$

where $[\cdot]^{\text{u}}$ indicates an average over all ascent regimes, $[\cdot]^{\text{d}}$ is an average over all descent regimes, and $[\delta T]^{g}$ is the global-mean surface-air temperature change as before. The dynamic component of the cloud feedback is decomposed into area and mix components in a similar way. Applying the decomposition (8) to the dynamics feedback (and estimating the area and mix components using least-squares regression, as discussed above), we find that the area and mix components both contribute to the all-sky and cloud dynamics feedbacks (Fig. 6). For the all-sky feedback, the area and mix components are both positive in the deep tropics (Fig. 6a) and contribute approximately equally to the strong positive dynamics feedback in that region. These positive contributions to the dynamics feedback in the deep tropics are a result of a strengthening of upward motion within ascending regions (mix component) and small increases in the ascending area within the ITCZ (area component). On the equatorward flanks of the ITCZ, the area component is a weak negative feedback reflecting atmospheric drying and reduced shortwave absorption and longwave greenhouse effect due to the narrowing of the ITCZ. Both the area and mix components decay

in magnitude moving away from the equator. Interestingly, the mix component dominates the dynamic component of the cloud feedback (Fig. 6b).

Overall, the influence of changes in the tropical up-down area ratio on climate feedbacks is weak compared to the influence of thermodynamic processes (cf. Fig. 2). This result contrasts with the findings of Pierrehumbert (1995) based on a simple two-box model of the tropical climate, and casts doubt on the ability of changes in the widths of the ITCZ or Hadley circulation to strongly influence global climates of the past or the future.

4) Size of the nonlinear component

We found that the nonlinear components of the radiative feedbacks are small relative to the dynamic and thermodynamic components (Fig. 2). However, it is interesting to consider the factors controlling the magnitudes of these nonlinear terms. To gain insight into the nonlinear components of the all-sky and cloud feedbacks [(6) and (7)], it is instructive to assume the relationship between TOA radiation and vertical velocity is linear, i.e., $R(\omega) = a + b\omega$ (here for convenience R represents either R_{all} or R_{cloud}). The assumption of linearity is reasonable in climate models over the majority of tropical vertical-velocity regimes for both the cloud-radiative effect (Fig. 1a) and clear-sky fluxes (Fig. 1b). Taking the definitions of the dynamic and nonlinear components of the all-sky radiative response (4) or changes in cloud-radiative effect (5), substituting in $R(\omega) = a + b\omega$ and rearranging, the ratio of the nonlinear component to the dynamic component can be shown to be equal to $\delta b/b$, where δb in this case denotes the change in the slope of the linear fit to $R(\omega)$ between the *piControl* and *abrupt4xCO2* runs. For the cloud-radiative effect, $\delta b/b \approx -20\%$ meaning that the sensitivity of the cloud-radiative effect to changes in mid-tropospheric vertical velocity decreases by 20% under global warming in the simulations analyzed here. This weakening of the relationship between vertical velocity and cloud-radiative effect as the climate warms

could be a result of cloud-masking effects associated with rising CO_2 and water-vapor concentrations in the atmosphere, and it also suggests that mid-tropospheric vertical velocity alone is not a good predictor of cloud changes. Our simple analysis suggests that the nonlinear component of changes in cloud-radiative effect (or the nonlinear component of the all-sky radiative response) is approximately 20% of the magnitude of the dynamic component, which roughly matches the nonlinear feedbacks calculated explicitly using the decompositions [(6) and (7)] (cf. Figure 2).

b. Global atmospheric dynamics feedback

Averaged over all latitudes, TOA radiative anomalies induced by CO_2 quadrupling are mostly a result of thermodynamic processes (see the results for one representative climate model in Figure 7). Although the atmospheric dynamics feedback is relatively important at low latitudes (Fig. 2a), there is a large degree of cancellation between positive and negative dynamics feedbacks when the global average is calculated. In what follows, we explain why the atmospheric dynamics feedback is small when averaged over large regions.

1) MASS BUDGET CONSTRAINT

That the global atmospheric dynamics feedback is small is perhaps not surprising when the constraint of the atmospheric mass budget is taken into account. Within a region that has a negligible net atmospheric mass flux across its lateral boundaries, such as the globe or the region occupied by the Hadley circulation, the steady-state atmospheric mass budget can be expressed as:

$$\int_{-\infty}^{0} \omega A(\omega) d\omega = -\int_{0}^{\infty} \omega A(\omega) d\omega, \tag{9}$$

where $A(\omega)$ here is the normalized area PDF of vertical velocity defined for the specified region (e.g., the globe). Expression (9) stipulates that in the steady-state atmosphere, the area of upward motion multiplied by the average upward velocity is equal to the area of downward motion

multiplied by the average downward velocity. We now illustrate how this mass budget places a strong constraint on the ability of changes in the atmospheric circulation to influence global TOA radiation and climate.

As in our discussion of the nonlinear component above, a useful starting point is to assume the dependence of TOA radiation (either the all-sky radiative response or the cloud-radiative effect) on mid-tropospheric vertical velocity is linear, i.e., $R(\omega) = a + b\omega$. Linearity is not an unreasonable assumption for climate models, at least for tropical vertical-velocity regimes with a heavy area weighting (Fig. 1). The linearity assumption is also supported by satellite observations of the cloud-radiative effect (Wyant et al. 2006). Using this assumption, the dynamic components of (4) or (5) are given by: $\int_{-\infty}^{\infty} R(\omega)\delta A(\omega)d\omega = a\int_{-\infty}^{\infty}\delta A(\omega)d\omega + b\int_{-\infty}^{\infty}\omega\delta A(\omega)d\omega$. By construction of normalized area PDFs, $\int_{-\infty}^{\infty}\delta A(\omega)d\omega = 0$, and from the atmospheric mass budget (9) it follows that $\int_{-\infty}^{\infty}\omega\delta A(\omega)d\omega = 0$. Consequently, for a strictly linear relationship between TOA radiation and vertical velocity, the impact of changes in atmospheric circulation on TOA radiative anomalies averaged over a closed-mass region is expected to be zero. A slightly modified argument can be used to show that the nonlinear components of (4) and (5) are also zero for linear $R(\omega)$. The implications of a linear $R(\omega)$ for the dynamic component of changes in cloud-radiative effect have been discussed previously by Wyant et al. (2006).

2) Effect on global climate change

Although small in magnitude, the globally-averaged atmospheric dynamics feedback nevertheless has an influence on the climate response to CO_2 quadrupling (Figs. 7 and 8). For the equilibrium climate response (ECR), defined here as the equilibrium change in near-surface temperature following CO_2 quadrupling calculated using the regression method of Gregory et al. (2004), the dynamics feedback marginally increases the surface warming (Figs. 7 and 8a) – the multimodel-

mean ECR is approximately 0.5 K larger than that predicted by the thermodynamics feedback alone (0.5 K corresponds to 8% of the multimodel-mean ECR in these simulations). Interestingly, the global dynamics feedback is robustly *positive* across CMIP5 models (Fig. 8). This contrasts with the hypothesis that tropical circulation changes may be a *negative* iris-type feedback on climate change (e.g., Lindzen et al. 2001). Despite being a small and positive feedback on climate change, there is no correlation between the all-sky dynamics feedback (globally averaged) and ECR, indicating that differences in atmospheric circulation responses across models cannot be used to explain intermodel spread in ECR. In contrast, there is a strong correlation of $r = 0.83$ between the thermodynamics feedbacks and ECRs across models.

The global feedback parameter, or the slope of the linear regression of the all-sky radiative response versus near-surface temperature anomalies, describes the efficiency with which the Earth system equilibrates a radiative forcing. The feedback parameter is the sum of all the individual feedback processes (e.g., water vapor, cloud, lapse rate) and is typically negative, meaning that the net downward flux of radiation at TOA decreases as the surface temperature increases during equilibration. The atmospheric dynamics feedback robustly makes the global feedback parameter less negative (Figs. 7 and 8b), implying that the Earth system is less efficient at eliminating a TOA forcing because of circulation changes. This reduction in the magnitude of the feedback parameter is consistent with the all-sky radiative response associated with circulation changes becoming less negative over time following CO_2 quadrupling (Figs. 5a and 7).

The climate models examined here are unable to simulate processes such as convective aggregation that have been put forward as potentially important influencers of global climate (Bony et al. 2016). Furthermore, climate models struggle to accurately simulate clouds (Pincus et al. 2008), and it is plausible that important nonlinearities in the $R_{\mathrm{all}}(\omega,\phi)$ and $R_{\mathrm{cloud}}(\omega,\phi)$ relationships, not captured by climate models, could lead to dynamics feedbacks that are substantially non-zero on

global scales. In the next section we will use an idealized GCM with prescribed TOA forcings to investigate how large atmospheric dynamics feedbacks, potentially induced by the effects mentioned above but not simulated by the current generation of climate models, could influence global climate.

4. Effectiveness of high- versus low-latitude dynamics feedbacks

a. Idealized forcing simulations

We use a moist idealized GCM perturbed by stylized TOA longwave forcing profiles to investigate in a general way how the latitudinal structure of the atmospheric dynamics feedback could impact global climate. Simulations are performed using the slab-ocean aquaplanet GCM of O'Gorman and Schneider (2008), which is based upon the model of Frierson et al. (2006) and Frierson (2007). The GCM is run at a horizontal spectral resolution of T42 with 10 vertical levels and the surface heat capacity is equivalent to 1m of liquid water. The model uses a simplified two-stream gray radiation scheme with a prescribed longwave optical thickness; shortwave fluxes are specified as a function of latitude and longitude [see O'Gorman and Schneider (2008) for full details of the radiation scheme]. It is important to note that this model does not simulate water-vapor or cloud feedbacks.

We perform a control simulation (without TOA longwave forcing) that has a climate roughly similar to that of the present-day Earth, along with three perturbed simulations with prescribed longwave forcings (Fig. 9a): A tropical forcing from $\phi = -30^\circ$ to 30° and an extratropical forcing ($\phi = -90^\circ$ to -30° and $\phi = 30^\circ$ to 90°), both with a global-mean forcing of $4\,\mathrm{W\,m^{-2}}$, and a global wave forcing with a maximum amplitude of $4\,\mathrm{W\,m^{-2}}$ and a global mean of $0\,\mathrm{W\,m^{-2}}$. Each forcing has a $\cos 3\phi$ dependence on latitude and is invariant with longitude. To prescribe the TOA

longwave forcings, we simply impose longwave radiative fluxes (positive downward) at the top level of the model with patterns as shown in Figure 9a. Each simulation is spun up for 1000 days with averages taken over the subsequent 2000 days. The magnitudes of the stylized forcings are considerably larger than what we have calculated for the dynamic component of the all-sky radiative response in the fully-coupled simulations (cf. Fig. 5), and the latitudinal structures imposed here are also highly idealized. However, our objective is to understand the effectiveness of high-latitude versus low-latitude TOA anomalies (due to changes in atmospheric circulation) in changing global climate, and for this purpose using an idealized GCM and stylized forcings is an appropriate first step.

b. Surface temperature responses

Although the tropical and extratropical forcings have equal magnitudes in the global mean, they induce strikingly different surface temperature responses (Fig. 9b). The global temperature response to extratropical forcing (1 K) is greater than twice the magnitude of the response to tropical forcing (0.4 K). This stronger sensitivity of climate to extratropical versus tropical forcing has also been shown for surface forcings (Rose et al. 2014; Rugenstein et al. 2016) – ocean heat uptake at high latitudes cools the climate more efficiently than the same heat uptake at low latitudes. The difference in temperature responses between low- and high-latitude forcings (a factor of approximately 2) found in our idealized simulations is somewhat smaller than for full-physics simulations forced by ocean heat uptake patterns (a factor of approximately 3–4; Rose et al. 2014). The enhanced contrast in global temperature responses for high- versus low-latitude forcings in full-physics simulations (Rose et al. 2014) relative to the idealized simulations is due to the full-physics simulations including water-vapor and cloud feedbacks, which further strengthen differences in the forcing responses. To further emphasize how the latitudinal pattern of TOA forcing

influences global temperature, the global-wave forcing has a global-mean magnitude of zero (Fig. 9a) and yet induces a surface-temperature cooling of 0.2 K. That the global-mean temperature can change in response to a forcing with latitudinal structure but zero global mean has been shown in previous studies (e.g., Rose and Ferreira 2013; Rose and Rencurrel 2016).

The physical mechanisms leading to the enhanced global climate response to high-latitude versus low-latitude forcings have received considerable attention (e.g., Hansen et al. 1997; Langen and Alexeev 2007; Lu and Cai 2010; Pithan and Mauritsen 2014; Rose et al. 2014; Roe et al. 2015). Fundamentally, the contrasting temperature responses are driven by different sensitivities of poleward atmospheric energy transport to high-latitude and low-latitude temperature perturbations, as well as latitudinal variations in local radiative feedbacks [see Rose et al. (2014) for an insightful discussion on this topic]. Consequently, although the idealized GCM used here omits a variety of processes which might be expected to change the magnitude of the climate response to TOA forcing (e.g., water-vapor and ice-albedo feedbacks), we believe the larger climate sensitivity to high-latitude forcing is a robust result that is grounded in well-established physical mechanisms. It should be noted that despite global surface temperature being more sensitive to a $1\,\mathrm{W\,m^{-2}}$ forcing prescribed at high latitudes versus at low latitudes, the equilibrium climate sensitivity in CMIP5 models and its inter-model spread is dominated by tropical forcings and feedbacks because the tropics makes up a large fraction of Earth's total area and because cloud feedbacks are more uncertain across models in the tropics than at higher latitudes (Vial et al. 2013).

The idealized simulations discussed in this section have important implications for the atmospheric dynamics feedback. Although the influence of circulation changes on Earth's global radiative balance is constrained to be weak as discussed above, the effect of circulation changes on the TOA radiative response at different latitudes is non-negligible (Fig. 2a), and the global temperature response to circulation changes is likely to depend on this latitudinal structure. Furthermore, dis-

cussions of how the atmospheric circulation response might mitigate climate change have focused largely on tropical iris-type mechanisms (e.g., Pierrehumbert 1995; Lindzen et al. 2001; Mauritsen and Stevens 2015; Bony et al. 2016). However, based on the idealized simulations presented here, a $10\,\mathrm{W\,m^{-2}}$ tropical TOA forcing would be needed to change global temperature by 1 K (a more realistic model with water-vapor and cloud feedbacks would be expected to require a smaller TOA forcing to change global temperature by 1 K, as discussed above). Our analysis of the influence of atmospheric dynamics on TOA radiation in CMIP5 models suggests a circulation-induced tropical TOA radiative anomaly of no greater than 1–$2\,\mathrm{W\,m^{-2}}$ under CO_2 quadrupling (Fig. 5a), which would have only a minor influence on global temperature. Furthermore, an observational analysis shows that convective aggregation also has only a weak influence on TOA radiation [of order $1\,\mathrm{W\,m^{-2}}$ (Tobin et al. 2012)]. Consequently, we argue that the relative insensitivity of global temperature to tropical TOA perturbations, combined with these perturbations due to changes in the atmospheric circulation being constrained to be small on large scales, means that tropical iris-type mechanisms are unlikely to exert a substantial influence on past or future climate change.

5. Summary and discussion

The response of the atmospheric circulation to radiative forcing, via its influence on clouds and water vapor, has been put forward as a potentially important negative feedback on climate change (Lindzen et al. 2001). Here, using a method based on that of Bony et al. (2004), we have calculated for the first time the atmospheric dynamics feedback at each latitude in a range of climate models subjected to an abrupt CO_2 quadrupling. For the all-sky feedback, the dynamic component is generally smaller than the thermodynamic component, though is not entirely negligible, particularly in the tropics, where it is positive with a magnitude of approximately $0.5\,\mathrm{W\,m^{-2}\,K^{-1}}$. For the cloud feedback, the dynamic component is comparable to the thermodynamic component

close to the equator. The latitudinal pattern of the dynamics feedback reflects previously identified changes in the tropical circulation under global warming including enhanced ascent in the core of the ITCZ and a narrowing of this convergence zone. This coupling between radiation and circulation emphasizes the necessity of understanding the sensitivity of large-scale atmospheric dynamics to climate change in order to fully understand climate feedbacks at low latitudes.

At individual latitudes in the tropics, the atmospheric dynamics feedback is comparable to the thermodynamics feedback. However, a large degree of cancellation between positive and negative dynamics feedbacks at different latitudes results in the thermodynamic component dominating the global climate response. That the global-mean atmospheric dynamics feedback is small is shown to be a consequence of (i) the steady-state atmospheric mass budget and (ii) approximately linear relationships between mid-tropospheric vertical velocity and the cloud-radiative effect and all-sky fluxes, though these relationships between vertical velocity and radiation require further investigation in high-resolution simulations that permit clouds and explicitly simulate convection. This atmospheric-mass constraint on the dynamics feedback raises doubts regarding the ability of iris-type mechanisms (e.g., convective aggregation) to limit future climate change.

Although the global radiative anomalies induced by circulation changes are small relative to anomalies induced by thermodynamic processes (e.g., temperature-driven changes in water vapor), they do affect the climate response to CO_2 quadrupling. Circulation changes are a positive feedback on global climate change (in contrast to iris-type negative feedbacks) and make the Earth system less efficient at equilibrating an imposed radiative forcing. Specifically, the dynamics feedback increases the multimodel-mean ECR by 0.5 K (or approximately 8% of the total warming) relative to a calculation of ECR using the thermodynamics feedback alone.

We performed idealized simulations to assess how hypothetical circulation-induced TOA anomalies at low and high latitudes, such as those due to unresolved dynamical processes includ-

ing convective aggregation, could affect global climate. We showed that a high-latitude forcing is twice as effective as a low-latitude forcing in changing global surface temperature (interestingly and in agreement with previous studies, we also found that a forcing with a global average of zero can induce a non-zero temperature response). These results further strengthen our argument that low-latitude dynamical responses to climate change – such as convective aggregation or ITCZ narrowing – are unlikely to greatly influence global climate unless they are capable of inducing very large TOA anomalies. On the other hand, circulation changes that create TOA anomalies at higher latitudes (for example poleward shifts in the storm tracks or deflections of the mid-latitude jet by large continental ice sheets in cold climates) are expected to be more than twice as effective at changing global temperature and consequently should be a priority to understand and quantify.

Our findings suggest a number of avenues for future research. Decades of satellite measurements now enable observational estimates of the atmospheric dynamics feedback; such estimates would be a useful benchmark with which to assess our climate-model results. These observations could also be examined in detail to assess whether non-linearities in observed $R_{\mathrm{all}}(\omega,\phi)$ and $R_{\mathrm{cloud}}(\omega,\phi)$ relationships are sufficiently strong to generate atmospheric dynamics feedbacks that could strongly influence global climate. We have considered here the effect of changes in resolved dynamical processes on climate in global models, but it would also be insightful to perform similar analyses in high-resolution convection-permitting simulations to assess how small-scale dynamical processes couple to TOA radiation. Our focus has been the influence of atmospheric circulation changes on TOA radiation and global temperature. However, the global precipitation response to climate change is linked to TOA as well as to surface radiation (e.g., O'Gorman et al. 2012). An interesting topic for future work would be to understand the contribution of circulation changes to the atmospheric (rather than to the TOA) radiation budget and consequently to the response of global precipitation to climate change (Su et al. 2017).

Acknowledgments. We thank Paulo Ceppi, Reto Knutti, Paul O'Gorman, Brian Rose, Maria Rugenstein, and the Editor for helpful comments, suggestions, and discussions. M.P.B. acknowledges support from the Imperial College London Research Fellowship Scheme.

References

Allan, R. P., 2011: Combining satellite data and models to estimate cloud radiative effect at the surface and in the atmosphere. *Meteorological Applications*, **18**, 324–333.

Andrews, T., J. M. Gregory, M. J. Webb, and K. E. Taylor, 2012: Forcing, feedbacks and climate sensitivity in CMIP5 coupled atmosphere-ocean climate models. *Geophys. Res. Lett.*, **39**, L09712.

Armour, K. C., C. M. Bitz, and G. H. Roe, 2013: Time-varying climate sensitivity from regional feedbacks. *J. Climate*, **26**, 4518–4534.

Bony, S., G. Bellon, D. Klocke, S. Sherwood, S. Fermepin, and S. Denvil, 2013: Robust direct effect of carbon dioxide on tropical circulation and regional precipitation. *Nat. Geosci.*, **6**, 447–451.

Bony, S., and J. L. Dufresne, 2005: Marine boundary layer clouds at the heart of tropical cloud feedback uncertainties in climate models. *Geophys. Res. Lett.*, **32**, L20806.

Bony, S., J.-L. Dufresne, H. Le Treut, J.-J. Morcrette, and C. Senior, 2004: On dynamic and thermodynamic components of cloud changes. *Climate Dyn.*, **22**, 71–86.

Bony, S., K. M. Lau, and Y. C. Sud, 1997: Sea surface temperature and large-scale circulation influences on tropical greenhouse effect and cloud radiative forcing. *J. Climate*, **10**, 2055–2077.

Bony, S., B. Stevens, D. Coppin, T. Becker, K. A. Reed, A. Voigt, and B. Medeiros, 2016: Thermodynamic control of anvil cloud amount. *Proc. Natl. Acad. Sci.*, **113**, 8927–8932.

Byrne, M. P., and P. A. O'Gorman, 2015: The response of precipitation minus evapotranspiration to climate warming: Why the "wet-get-wetter, dry-get-drier" scaling does not hold over land. *J. Climate*, **28**, 8078–8092.

Byrne, M. P., and T. Schneider, 2016a: Energetic constraints on the width of the intertropical convergence zone. *J. Climate*, **29**, 4709–4721.

Byrne, M. P., and T. Schneider, 2016b: Narrowing of the ITCZ in a warming climate: Physical mechanisms. *Geophys. Res. Lett.*, **43**, 11,350–11,357.

Ceppi, P., F. Brient, M. D. Zelinka, and D. L. Hartmann, 2017a: Cloud feedback mechanisms and their representation in global climate models. *WIREs Climate Change*, **8**, doi:10.1002/wcc.465.

Ceppi, P., G. Zappa, T. G. Shepherd, and J. M. Gregory, 2017b: Fast and slow components of the extratropical atmospheric circulation response to CO_2 forcing. *J. Climate*, doi:10.1175/JCLI-D-17-0323.1.

Cronin, T. W., and A. A. Wing, 2017: Clouds, circulation, and climate sensitivity in a radiative-convective equilibrium channel model. *J. Adv. Model. Earth Syst.*, doi:10.1002/2017MS001111.

Frierson, D. M. W., 2007: The dynamics of idealized convection schemes and their effect on the zonally averaged tropical circulation. *J. Atmos. Sci.*, **64**, 1959–1976.

Frierson, D. M. W., I. M. Held, and P. Zurita-Gotor, 2006: A gray-radiation aquaplanet moist GCM. Part I: Static stability and eddy scale. *J. Atmos. Sci.*, **63**, 2548–2566.

Fu, Q., M. Baker, and D. L. Hartmann, 2002: Tropical cirrus and water vapor: an effective Earth infrared iris feedback? *Atmos. Chem. Phys.*, **2**, 31–37.

644 Gregory, J. M., and Coauthors, 2004: A new method for diagnosing radiative forcing and climate
645 sensitivity. *Geophys. Res. Lett.*, **31**, L03205.

646 Grise, K. M., L. M. Polvani, G. Tselioudis, Y. Wu, and M. D. Zelinka, 2013: The ozone hole
647 indirect effect: Cloud-radiative anomalies accompanying the poleward shift of the eddy-driven
648 jet in the Southern Hemisphere. *Geophys. Res. Lett.*, **40**, 3688–3692.

649 Hansen, J., M. Sato, and R. Ruedy, 1997: Radiative forcing and climate response. *J. Geophys.*
650 *Res.: Atmos.*, **102**, 6831–6864.

651 Hartmann, D. L., and K. Larson, 2002: An important constraint on tropical cloud-climate feed-
652 back. *Geophys. Res. Lett.*, **29**, doi:10.1029/2002GL015835, 1951.

653 Kamae, Y., M. Watanabe, T. Ogura, M. Yoshimori, and H. Shiogama, 2015: Rapid adjustments of
654 cloud and hydrological cycle to increasing CO_2: a review. *Curr. Clim. Change Rep.*, **1**, 103–113.

655 Kay, J. E., B. Medeiros, Y.-T. Hwang, A. Gettelman, J. Perket, and M. G. Flanner, 2014: Processes
656 controlling Southern Ocean shortwave climate feedbacks in CESM. *Geophys. Res. Lett.*, **41**,
657 616–622.

658 Langen, P. L., and V. A. Alexeev, 2007: Polar amplification as a preferred response in an idealized
659 aquaplanet GCM. *Climate Dyn.*, **29**, 305–317.

660 Lau, W. K. M., and K. M. Kim, 2015: Robust hadley circulation changes and increasing global
661 dryness due to CO_2 warming from CMIP5 model projections. *Proc. Natl. Acad. Sci.*, **112**, 3630–
662 3635.

663 Lindzen, R. S., M.-D. Chou, and A. Y. Hou, 2001: Does the Earth have an adaptive infrared iris?
664 *Bull. Amer. Meteor. Soc.*, **82**, 417–432.

Lu, J., and M. Cai, 2010: Quantifying contributions to polar warming amplification in an idealized coupled general circulation model. *Climate Dyn.*, **34**, 669–687.

Lu, J., G. A. Vecchi, and T. Reichler, 2007: Expansion of the Hadley cell under global warming. *Geophys. Res. Lett.*, **34**, L06805.

Mauritsen, T., and B. Stevens, 2015: Missing iris effect as a possible cause of muted hydrological change and high climate sensitivity in models. *Nat. Geosci.*, **8**, 346–351.

O'Gorman, P. A., R. P. Allan, M. P. Byrne, and M. Previdi, 2012: Energetic constraints on precipitation under climate change. *Surv. Geophys.*, **33**, 585–608.

O'Gorman, P. A., and T. Schneider, 2008: The hydrological cycle over a wide range of climates simulated with an idealized GCM. *J. Climate*, **21**, 5797–5806.

Pierrehumbert, R. T., 1995: Thermostats, radiator fins, and the local runaway greenhouse. *J. Atmos. Sci.*, **52**, 1784–1806.

Pincus, R., C. P. Batstone, R. J. P. Hofmann, K. E. Taylor, and P. J. Glecker, 2008: Evaluating the present-day simulation of clouds, precipitation, and radiation in climate models. *J. Geophys. Res.: Atmos.*, **113 (D14)**.

Pithan, F., and T. Mauritsen, 2014: Arctic amplification dominated by temperature feedbacks in contemporary climate models. *Nat. Geosci.*, **7**, 181–184.

Ramanathan, V. L. R. D., R. D. Cess, E. F. Harrison, P. Minnis, B. R. Barkstrom, E. Ahmad, D. Hartmann, and Coauthors, 1989: Cloud-radiative forcing and climate: Results from the Earth Radiation Budget Experiment. *Science*, **243**, 57–63.

Roe, G. H., N. Feldl, K. C. Armour, Y.-T. Hwang, and D. M. W. Frierson, 2015: The remote impacts of climate feedbacks on regional climate predictability. *Nat. Geosci.*, **8**, 135–139.

687 Rose, B. E. J., K. C. Armour, D. S. Battisti, N. Feldl, and D. D. B. Koll, 2014: The dependence of
688 transient climate sensitivity and radiative feedbacks on the spatial pattern of ocean heat uptake.
689 *Geophys. Res. Lett.*, **41**, 1071–1078.

690 Rose, B. E. J., and D. Ferreira, 2013: Ocean heat transport and water vapor greenhouse in a warm
691 equable climate: A new look at the low gradient paradox. *J. Climate*, **26**, 2117–2136.

692 Rose, B. E. J., and L. Rayborn, 2016: The effects of ocean heat uptake on transient climate sensi-
693 tivity. *Current Climate Change Reports*, **2**, 190–201.

694 Rose, B. E. J., and M. C. Rencurrel, 2016: The vertical structure of tropospheric water vapor:
695 comparing radiative and ocean-driven climate changes. *J. Climate*, **29**, 4251–4268.

696 Rugenstein, M. A. A., K. Caldeira, and R. Knutti, 2016: Dependence of global radiative feedbacks
697 on evolving patterns of surface heat fluxes. *Geophys. Res. Lett.*, **43**, 9877–9885.

698 Scheff, J., and D. Frierson, 2012: Twenty-first-century multimodel subtropical precipitation de-
699 clines are mostly midlatitude shifts. *J. Climate*, **25**, 4330–4347.

700 Schneider, T., P. A. O'Gorman, and X. J. Levine, 2010: Water vapor and the dynamics of climate
701 changes. *Rev. Geophys.*, **48**, RG3001.

702 Seager, R., N. Naik, and G. A. Vecchi, 2010: Thermodynamic and dynamic mechanisms for
703 large-scale changes in the hydrological cycle in response to global warming. *J. Climate*, **23**,
704 4651–4668.

705 Shepherd, T. G., 2014: Atmospheric circulation as a source of uncertainty in climate change
706 projections. *Nat. Geosci.*, **7**, 703–708.

707 Soden, B. J., A. J. Broccoli, and R. S. Hemler, 2004: On the use of cloud forcing to estimate cloud
708 feedback. *J. Climate*, **17**, 3661–3665.

709 Su, H., and Coauthors, 2017: Tightening of tropical ascent and high clouds key to precipitation
710 change in a warmer climate. *Nat. Communications*, **8**, doi:10.1038/ncomms15771.

711 Taylor, K. E., R. J. Stouffer, and G. A. Meehl, 2012: An overview of CMIP5 and the experiment
712 design. *Bull. Amer. Meteor. Soc.*, **93**, 485–498.

713 Tobin, I., S. Bony, and R. Roca, 2012: Observational evidence for relationships between the degree
714 of aggregation of deep convection, water vapor, surface fluxes, and radiation. *J. Climate*, **25**,
715 6885–6904.

716 Vecchi, G. A., and B. J. Soden, 2007: Global warming and the weakening of the tropical circula-
717 tion. *J. Climate*, **20**, 4316–4340.

718 Vial, J., J.-L. Dufresne, and S. Bony, 2013: On the interpretation of inter-model spread in CMIP5
719 climate sensitivity estimates. *Climate Dyn.*, **41**, 3339–3362.

720 Wall, C. J., and D. L. Hartmann, 2015: On the influence of poleward jet shift on shortwave cloud
721 feedback in global climate models. *J. Adv. Model. Earth Syst.*, **7**, 2044–2059.

722 Wing, A. A., K. Emanuel, C. E. Holloway, and C. Muller, 2017: Convective self-aggregation in
723 numerical simulations: A review. *Surv. Geophys.*, 1–25, doi:10.1007/s10712-017-9408-4.

724 Wing, A. A., and K. A. Emanuel, 2014: Physical mechanisms controlling self-aggregation of
725 convection in idealized numerical modeling simulations. *J. Adv. Model. Earth Syst*, **6**, 59–74.

726 Wodzicki, K. R., and A. D. Rapp, 2016: Long-term characterization of the Pacific ITCZ using
727 TRMM, GPCP, and ERA-Interim. *J. Geophys. Res.: Atmos.*, **121**, 3153–3170.

728 Wyant, M. C., C. S. Bretherton, J. T. Bacmeister, J. T. Kiehl, I. M. Held, M. Zhao, S. A. Klein, and
729 B. J. Soden, 2006: A comparison of low-latitude cloud properties and their response to climate

change in three AGCMs sorted into regimes using mid-tropospheric vertical velocity. *Climate Dyn.*, **27**, 261–279.

Yin, J. H., 2005: A consistent poleward shift of the storm tracks in simulations of 21st century climate. *Geophys. Res. Lett.*, **32**, L18701.

Zelinka, M. D., S. A. Klein, and D. L. Hartmann, 2012: Computing and partitioning cloud feedbacks using cloud property histograms. Part II: Attribution to changes in cloud amount, altitude, and optical depth. *J. Climate*, **25**, 3736–3754.

LIST OF FIGURES

Fig. 1. The annual-mean TOA tropical (averaged from $\phi = -30^\circ$ to 30°, where ϕ is the latitude) (a) cloud-radiative effect, (b) clear-sky radiative flux, (c) all-sky radiative flux, and (d) normalized area PDF of vertical velocity, as a function of vertical velocity, for one climate model (MRI-CGCM3). The cloud-radiative effect is defined in the main text following Allan (2011), and the clear-sky and all-sky fluxes are specified to be positive downwards. For the cloud-radiative effect and the clear-sky and all-sky fluxes, red and blue lines indicate the shortwave and longwave components, respectively. Each dot represents a different vertical-velocity bin. The functions are constructed for each climatological month using vertical velocities and radiative fluxes averaged over 100 years of the *piControl* simulation, before the annual means are taken. The shortwave and longwave components of the clear-sky and all-sky fluxes have had their averages over all vertical velocity bins removed so as to emphasize the functional dependence on vertical velocity. 38

Fig. 2. Multimodel-mean total (a) all-sky and (b) cloud feedbacks versus latitude (black lines) in the *abrupt4xCO2* simulations. The thermodynamic (blue lines) and the dynamic components (red solid lines) of the feedbacks are also plotted, along with the nonlinear components (red dashed lines). Each total feedback and component has been estimated using least-squares regression over the first 100 years of the *abrupt4xCO2* simulations. In this figure and in all subsequent figures in which quantities are plotted as a function of latitude, each term has been multiplied by a factor of $\cos\phi$ to reflect the decreasing area per degree latitude towards the poles. 39

Fig. 3. Multimodel-mean change in (minus) the mid-tropospheric vertical velocity (averaged from 400hPa to 500hPa) between *piControl* and *abrupt4xCO2* runs (black line) along with (minus) the multimodel-mean vertical velocity from *piControl* (red line), which has been rescaled by a factor of 0.15. For both the climatological vertical velocity and the change in vertical velocity, 100-year averages are computed from the *piControl* and *abrupt4xCO2* runs. The vertical red dotted lines indicate the edges of the climatological ITCZ in *piControl*, where the ITCZ edges are defined as the latitudes closest to the equator at which the zonal-mean mid-tropospheric vertical velocity passes through zero (Byrne and Schneider 2016a). 40

Fig. 4. As in Figure 2 but here showing the dynamic components only (black lines) of the (a) all-sky and (b) cloud feedbacks. The shortwave (red lines) and longwave contributions (blue lines) to these dynamics feedbacks are also shown. 41

Fig. 5. Multimodel-mean dynamic + nonlinear components of the (a) all-sky radiative response and (c) changes in cloud-radiative effect, along with the thermodynamic components (b) and (d), between *piControl* and year 1 (red lines) and the averages over years 91-100 (black lines) of the *abrupt4xCO2* runs. 42

Fig. 6. Multimodel-mean dynamic + nonlinear components of the (a) all-sky and (b) cloud feedbacks in the *abrupt4xCO2* simulations (black lines). The "area" (red lines) and "mix" contributions (blue lines) to these dynamic + nonlinear components [as defined by (8)] are also shown. 43

Fig. 7. Global-mean TOA all-sky radiative anomalies for the CCSM4 model (black crosses) as a function of annual global-mean near-surface temperature changes for the first 100 years in the *abrupt4xCO2* simulation. The thermodynamic (blue dots) and dynamic + nonlinear components (red dots) of the anomalies are also shown (the diagnosed radiative forcing has been added to the thermodynamic component), along with ordinary least-squares fits to the

783 total anomalies (black solid line) and to the thermodynamic component of the anomalies
784 (blue dashed line). The estimated equilibrium climate responses (ECRs), based on the least-
785 squares fits, are also indicated. 44

786 **Fig. 8.** (a) Equilibrium climate response (ECR) and (b) global feedback parameter in the
787 *abrupt4xCO2* simulations for individual CMIP5 models (black open circles) and for the
788 multimodel mean (red solid circles). Both quantities are calculated using the regression
789 method of Gregory et al. (2004). The y-axes show the two quantities calculated using the
790 total TOA all-sky radiative responses (4), and the x-axes show the quantities calculated us-
791 ing only the thermodynamic components of the responses for each model (i.e. assuming a
792 fixed circulation). Hence, any departures from the one-to-one relationships (blue lines) in
793 the x-direction are due to changes in the atmospheric circulation [e.g., circulations changes
794 *increase* the multimodel-mean ECR as shown in panel (a)]. 45

795 **Fig. 9.** (a) Imposed longwave TOA forcings (positive downward) as a function of latitude for three
796 idealized simulations perturbed from a control run, and (b) the surface-temperature re-
797 sponses for each perturbed simulation relative to the control run. The black lines correspond
798 to the tropical forcing and induced response, the red lines to the extratropical forcing and
799 response, and the blue lines to the global-wave forcing and response. Each forcing has a
800 $\cos 3\phi$ functional form. 46

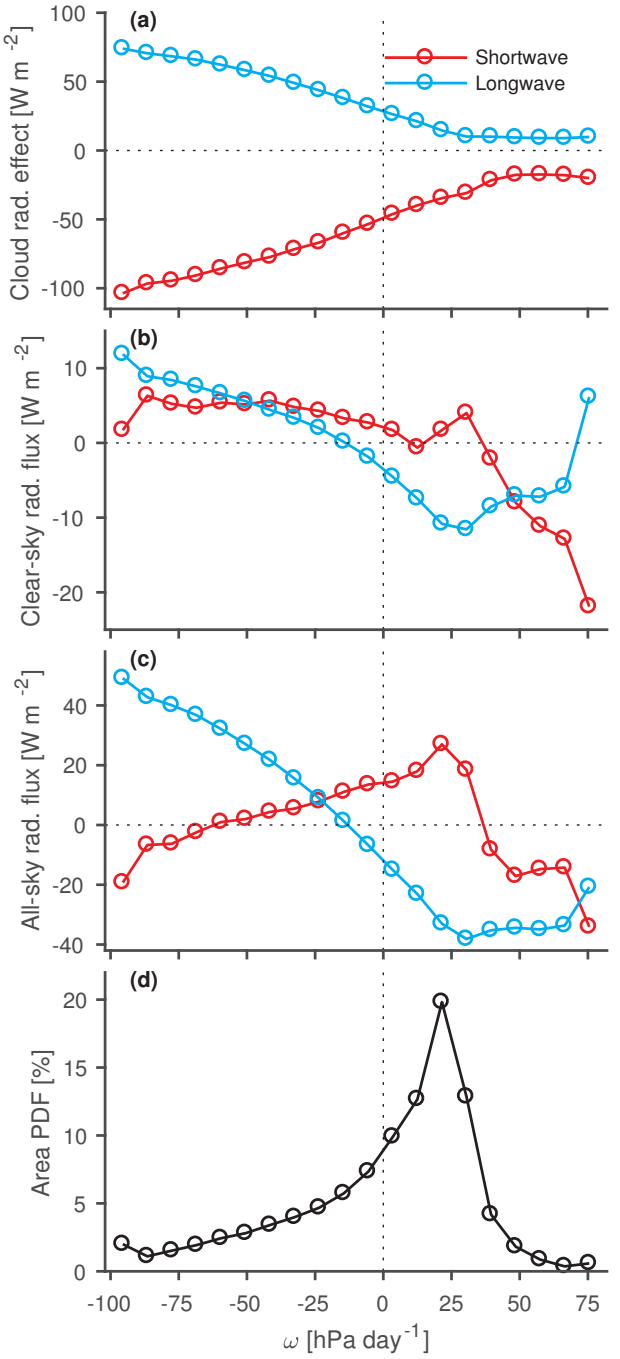

FIG. 1. The annual-mean TOA tropical (averaged from $\phi = -30°$ to $30°$, where ϕ is the latitude) (a) cloud-radiative effect, (b) clear-sky radiative flux, (c) all-sky radiative flux, and (d) normalized area PDF of vertical velocity, as a function of vertical velocity, for one climate model (MRI-CGCM3). The cloud-radiative effect is defined in the main text following Allan (2011), and the clear-sky and all-sky fluxes are specified to be positive downwards. For the cloud-radiative effect and the clear-sky and all-sky fluxes, red and blue lines indicate the shortwave and longwave components, respectively. Each dot represents a different vertical-velocity bin. The functions are constructed for each climatological month using vertical velocities and radiative fluxes averaged over 100 years of the *piControl* simulation, before the annual means are taken. The shortwave and longwave components of the clear-sky and all-sky fluxes have had their averages over all vertical velocity bins removed so

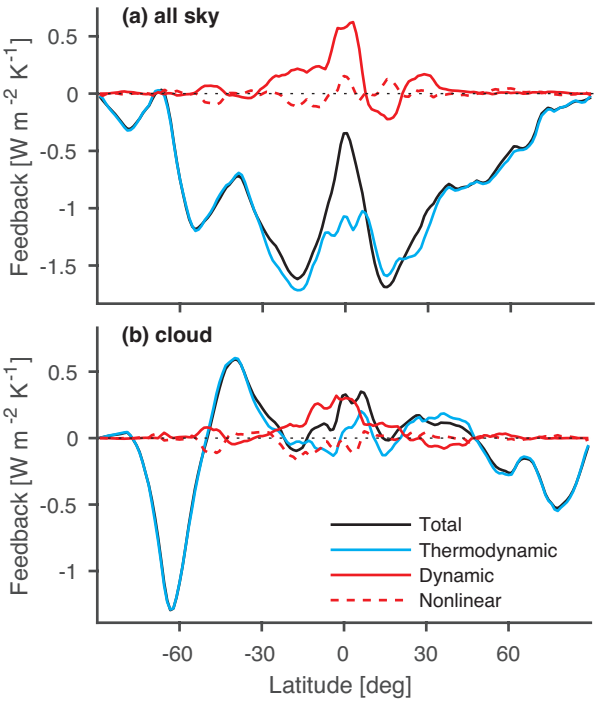

FIG. 2. Multimodel-mean total (a) all-sky and (b) cloud feedbacks versus latitude (black lines) in the *abrupt4xCO2* simulations. The thermodynamic (blue lines) and the dynamic components (red solid lines) of the feedbacks are also plotted, along with the nonlinear components (red dashed lines). Each total feedback and component has been estimated using least-squares regression over the first 100 years of the *abrupt4xCO2* simulations. In this figure and in all subsequent figures in which quantities are plotted as a function of latitude, each term has been multiplied by a factor of $\cos\phi$ to reflect the decreasing area per degree latitude towards the poles.

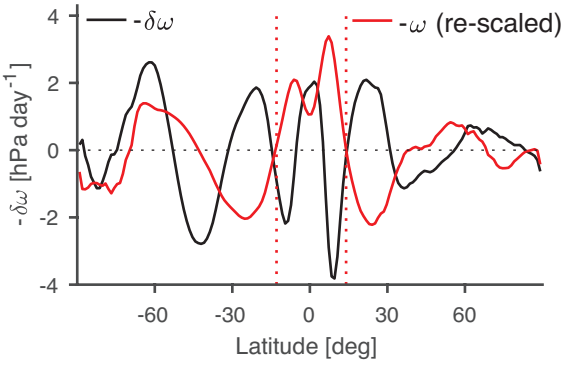

FIG. 3. Multimodel-mean change in (minus) the mid-tropospheric vertical velocity (averaged from 400hPa to 500hPa) between *piControl* and *abrupt4xCO2* runs (black line) along with (minus) the multimodel-mean vertical velocity from *piControl* (red line), which has been re-scaled by a factor of 0.15. For both the climatological vertical velocity and the change in vertical velocity, 100-year averages are computed from the *piControl* and *abrupt4xCO2* runs. The vertical red dotted lines indicate the edges of the climatological ITCZ in *piControl*, where the ITCZ edges are defined as the latitudes closest to the equator at which the zonal-mean mid-tropospheric vertical velocity passes through zero (Byrne and Schneider 2016a).

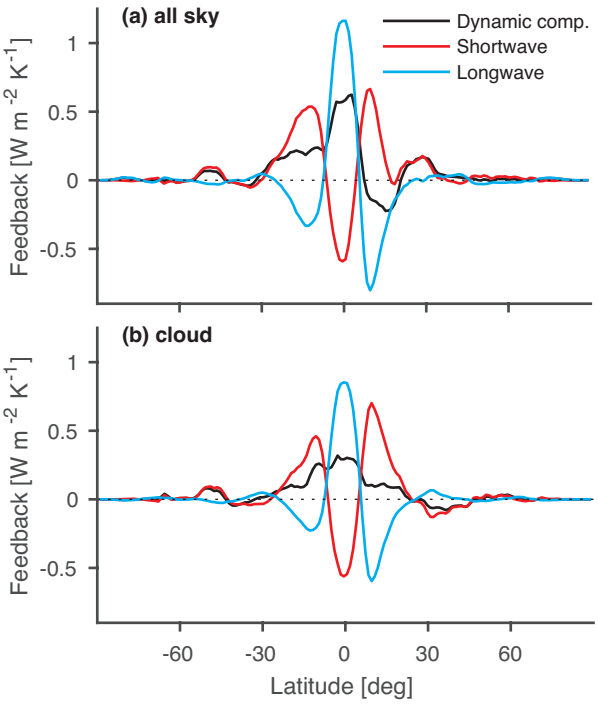

825 FIG. 4. As in Figure 2 but here showing the dynamic components only (black lines) of the (a) all-sky and (b)
826 cloud feedbacks. The shortwave (red lines) and longwave contributions (blue lines) to these dynamics feedbacks
827 are also shown.

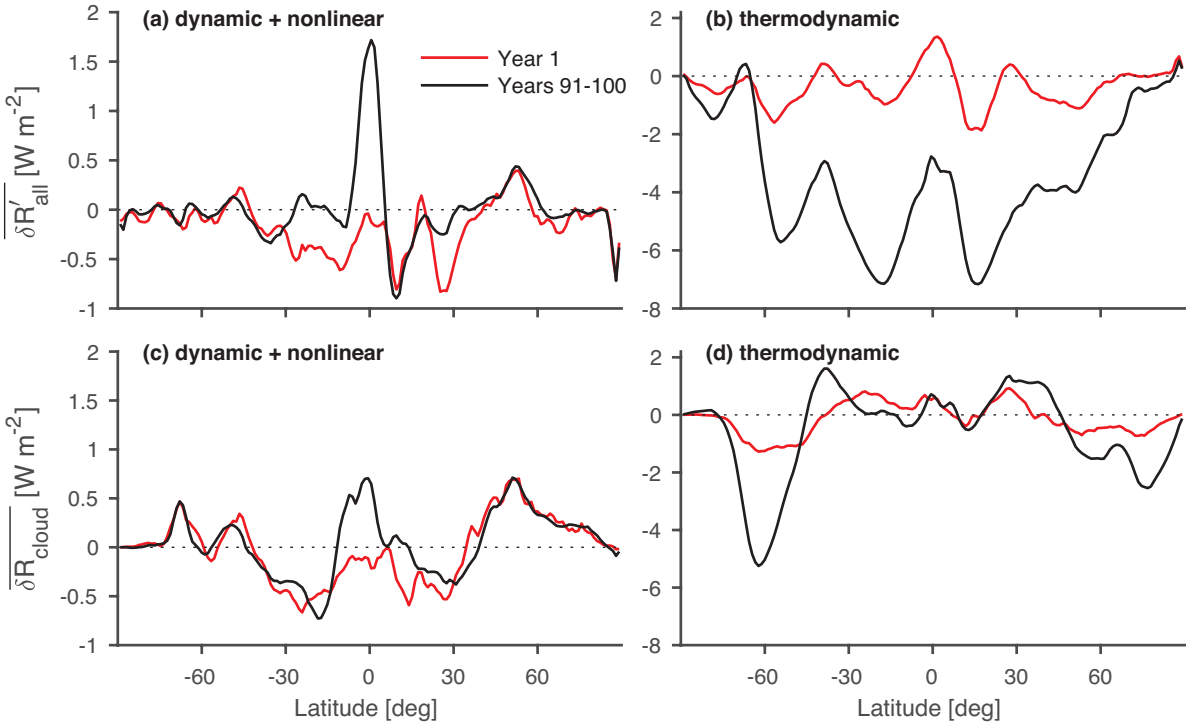

828 FIG. 5. Multimodel-mean dynamic + nonlinear components of the (a) all-sky radiative response and (c)
829 changes in cloud-radiative effect, along with the thermodynamic components (b) and (d), between *piControl*
830 and year 1 (red lines) and the averages over years 91-100 (black lines) of the *abrupt4xCO2* runs.

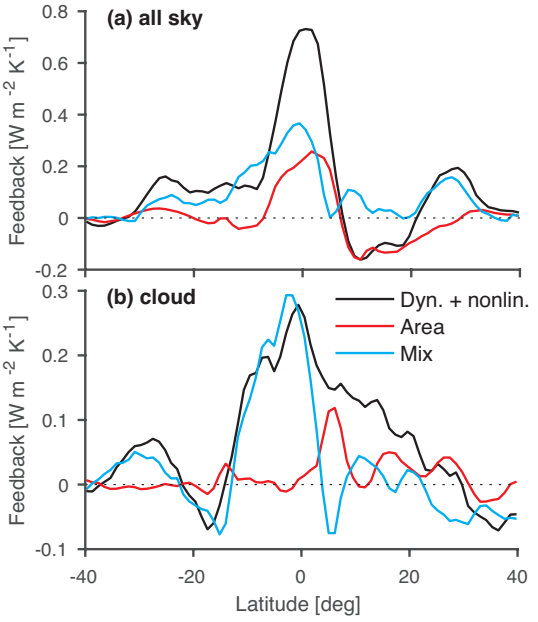

831 FIG. 6. Multimodel-mean dynamic + nonlinear components of the (a) all-sky and (b) cloud feedbacks in the
832 *abrupt4xCO2* simulations (black lines). The "area" (red lines) and "mix" contributions (blue lines) to these
833 dynamic + nonlinear components [as defined by (8)] are also shown.

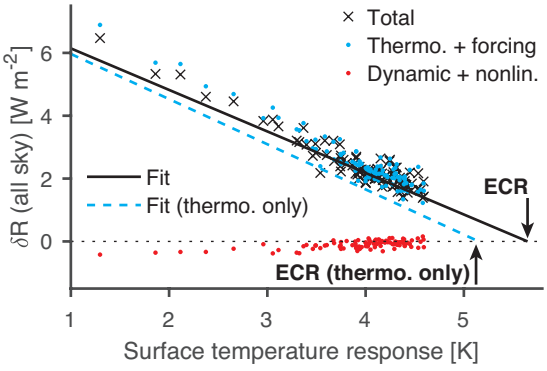

FIG. 7. Global-mean TOA all-sky radiative anomalies for the CCSM4 model (black crosses) as a function of annual global-mean near-surface temperature changes for the first 100 years in the *abrupt4xCO2* simulation. The thermodynamic (blue dots) and dynamic + nonlinear components (red dots) of the anomalies are also shown (the diagnosed radiative forcing has been added to the thermodynamic component), along with ordinary least-squares fits to the total anomalies (black solid line) and to the thermodynamic component of the anomalies (blue dashed line). The estimated equilibrium climate responses (ECRs), based on the least-squares fits, are also indicated.

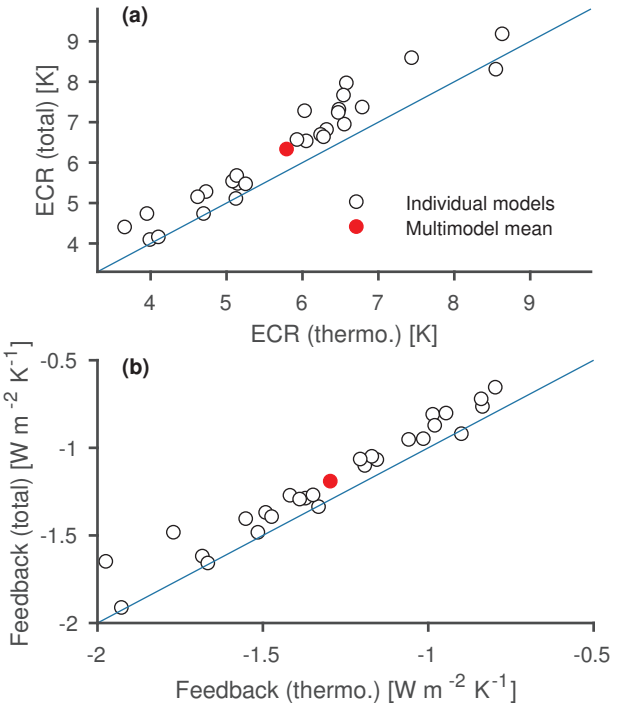

FIG. 8. (a) Equilibrium climate response (ECR) and (b) global feedback parameter in the *abrupt4xCO2* simulations for individual CMIP5 models (black open circles) and for the multimodel mean (red solid circles). Both quantities are calculated using the regression method of Gregory et al. (2004). The *y*-axes show the two quantities calculated using the total TOA all-sky radiative responses (4), and the *x*-axes show the quantities calculated using only the thermodynamic components of the responses for each model (i.e. assuming a fixed circulation). Hence, any departures from the one-to-one relationships (blue lines) in the *x*-direction are due to changes in the atmospheric circulation [e.g., circulations changes *increase* the multimodel-mean ECR as shown in panel (a)].

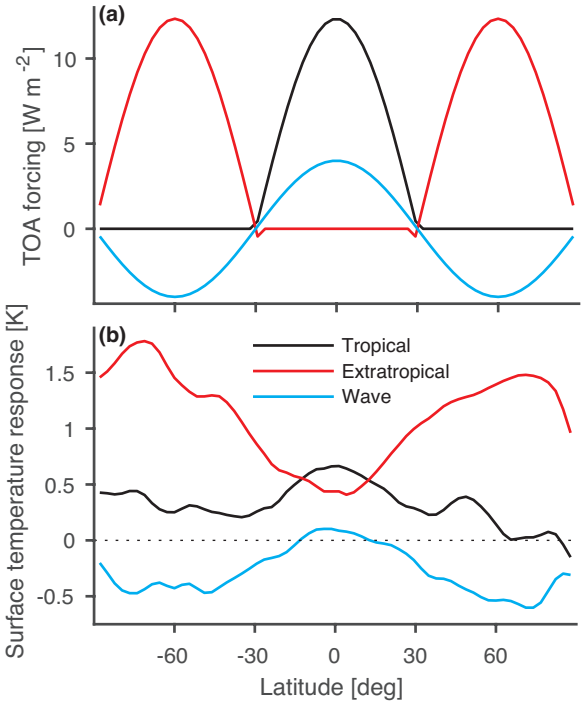

FIG. 9. (a) Imposed longwave TOA forcings (positive downward) as a function of latitude for three idealized simulations perturbed from a control run, and (b) the surface-temperature responses for each perturbed simulation relative to the control run. The black lines correspond to the tropical forcing and induced response, the red lines to the extratropical forcing and response, and the blue lines to the global-wave forcing and response. Each forcing has a $\cos 3\phi$ functional form.